Volume 16
Number 24
28 June 2025
Pages 10625–11166

Chemical Science

rsc.li/chemical-science

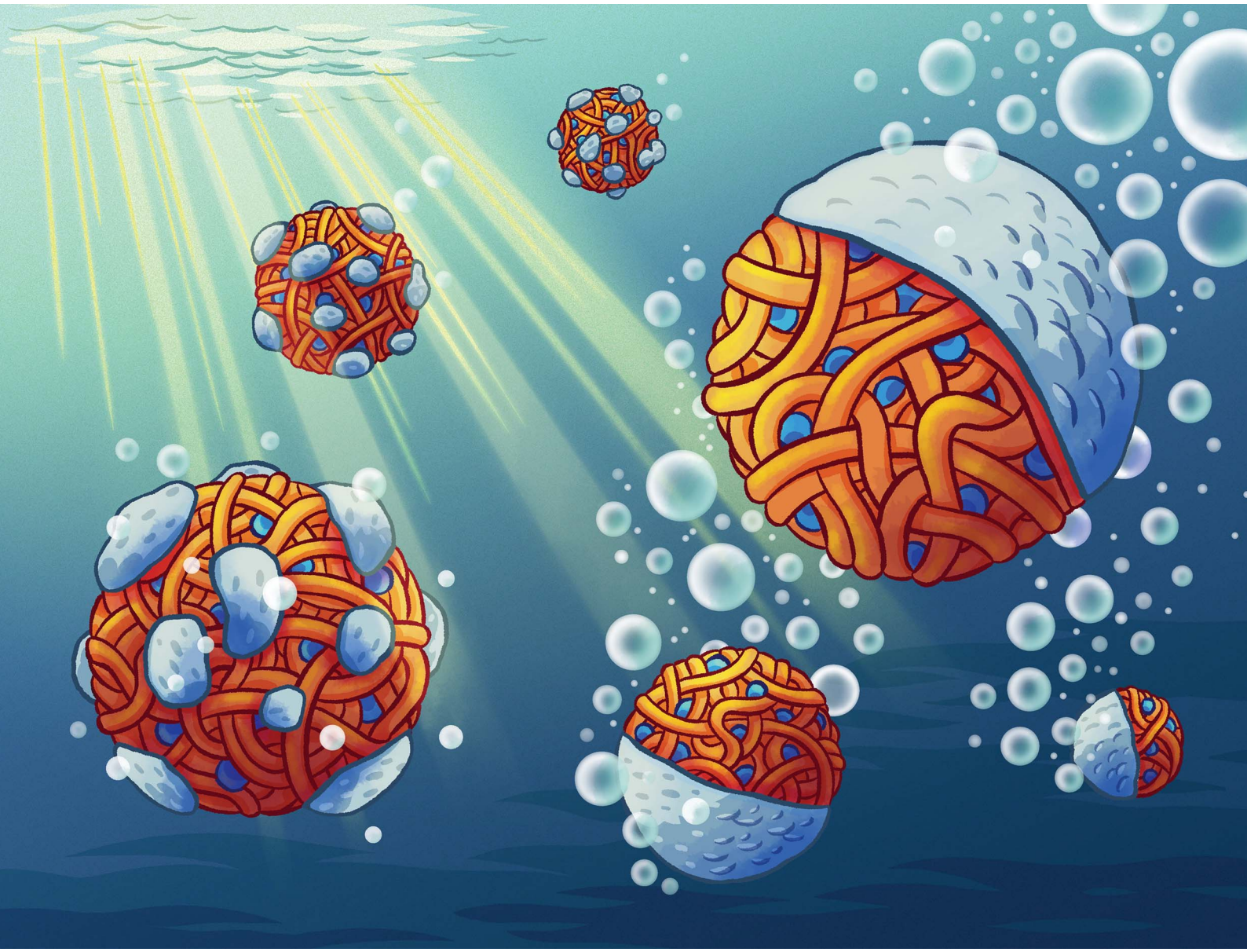

ISSN 2041-6539

ROYAL SOCIETY OF CHEMISTRY

EDGE ARTICLE
Sylvain Chambon, Alexander Kuhn *et al.*
Targeted design of organic Janus particles for improved photocatalytic hydrogen evolution

15 YEARS ANNIVERSARY

Chemical Science

ROYAL SOCIETY OF CHEMISTRY

EDGE ARTICLE

View Article Online
View Journal | View Issue

Cite this: *Chem. Sci.*, 2025, **16**, 10691

All publication charges for this article have been paid for by the Royal Society of Chemistry

Received 30th January 2025
Accepted 28th April 2025

DOI: 10.1039/d5sc00802f

rsc.li/chemical-science

Targeted design of organic Janus particles for improved photocatalytic hydrogen evolution†

Khaoula Missaoui,[a] Guillaume Wantz,[b] Thierry Toupance,[a] Sylvain Chambon *[b] and Alexander Kuhn *[a]

Organic bulk heterojunction particles are decorated in a well-controlled way with metals by using light-assisted bipolar electrodeposition to yield Janus particles. Their asymmetric character leads to significantly enhanced photocatalytic hydrogen evolution reaction. The organic particles are first synthesized *via* miniemulsion, tuning their size by carefully controlling various preparation parameters. Subsequently, the synergistic effect of an electric field and light is explored for the site-selective bipolar electrochemical deposition of different metals (Pt, Au or Pd). Photocatalytic tests reveal that in the case of platinum, the resulting Janus particles significantly outperform particles randomly covered with metal, as well as unmodified particles, showing an increase in hydrogen evolution efficiency by up to 500%. This superior performance is attributed to an enhanced charge carrier separation in the Janus structure, where Pt, confined at one side, facilitates more efficient electron shuttling and transfer. This work constitutes the first study reporting a promising approach for designing novel metal–organic Janus particles to boost photocatalytic hydrogen evolution and opens up new perspectives for optimizing the design of various other hybrid systems for sustainable energy conversion.

Introduction

To address the global challenges of energy deficiency and environmental change, extensive research has focused on the development of renewable energy sources.[1] As the most abundant renewable energy, solar power is a promising source to tackle the related scientific challenges. However, the intermittency of sunlight requires energy storage in the form of chemicals. In this context, hydrogen (H_2) is a clean fuel because it only produces electricity and water when used in fuel cells. Nowadays, chemical hydrogen production has been widely studied and the vast majority (>95%) of global hydrogen is produced from steam methane reforming, a process based on fossil fuel and also emitting large amounts of CO_2. In response to the environmental impact of these methods, photocatalytic water splitting for green hydrogen production, due to its low cost and environmental advantages, has emerged as a particularly hot topic in current research.[2,3] This process, which uses sunlight to split water into hydrogen and oxygen *via* semiconductor photocatalysts offers a method to directly convert solar energy into chemical fuels. However, to ensure scalability, this approach requires more efficient photocatalysts. Along with chemical and photochemical stability, the key requirements for an efficient system are: (i) solar light harvesting in a large wavelength window; (ii) efficient charge carrier separation after exciton generation; (iii) fast charge carrier transfer kinetics at the liquid–solid interface. In this context, inorganic semiconductor photocatalysts have been widely explored,[4,5] but may suffer from charge carrier recombination and light harvesting issues. On the other hand, hetero-nanostructures, combining different metal oxide semiconductors with metallic deposits have led to significant improvements with respect to charge carrier separation and transfer kinetics at the liquid–solid interface.[6,7] However, they often still show some limitations in terms of the active wavelength range, the overall solar-to-hydrogen conversion efficiency and the use of transition elements that could lead to sustainability issues.

As a consequence, systems capable of producing H_2 at a price competitive with fossil fuel-based H_2 production remain elusive. This challenge has driven the development of a new generation of organic semiconductors, based on both, conjugated polymer donors and small molecular acceptors. These stable materials show high performance and are already well-established ingredients of organic photovoltaic (OPV) devices.[8–10] The solar-to-electricity power conversion efficiency of state-of-the-art OPVs is now approaching 20% at the laboratory scale, achieved through the optimization of the molecular structures and advanced device engineering.[11,12] Considering the success of solution-processable organic semiconductors in OPV, research is now emerging to exploit their advantages also

[a]*Univ. Bordeaux, CNRS, Bordeaux INP, ISM UMR 5255, 33607 Pessac, France. E-mail: kuhn@enscbp.fr*

[b]*Univ. Bordeaux, CNRS, Bordeaux INP, IMS UMR 5218, 33607 Pessac, France. E-mail: sylvain.chambon@u-bordeaux.fr*

† Electronic supplementary information (ESI) available. See DOI: https://doi.org/10.1039/d5sc00802f

for solar-to-hydrogen conversion. Organic semiconductors, composed of earth-abundant elements, offer customizable optical bandgaps, energy levels, charge transport efficiencies and optoelectronic properties through molecular engineering.[13–15] This flexibility enables a fine-tuning of their properties, making them promising candidates for their use in solar water-splitting devices. These alternative photocatalysts include polymeric carbon nitride,[16] carbon dots,[17,18] conjugated microporous polymers,[19] and linear conjugated polymers.[20] However organic photocatalysts also have some inherent limitations, such as high exciton binding energies, low charge-carrier mobilities, and short charge migration distances.[21,22] In OPV, these challenges have been addressed through the use of donor/acceptor bulk heterojunctions. To ensure an efficient hydrogen evolution reaction (HER), it is therefore essential to focus on the molecular design of new organic semiconductors, the tailoring of the heterojunction, the optimization of the morphology and the improvement of exciton dissociation at the photocatalyst surface. Among others, this can be achieved by increasing the interfacial area between the n-type semiconductor and the electrolyte *via* tuning the particle morphology. In general, nanoscale mixtures of donor and acceptor materials also allow excitons to reach more easily the interface where they can dissociate into free charge carriers. Consequently, an analog approach can also be applied to organic polymer photocatalysts.

For the elaboration of organic photovoltaics devices, a donor and an acceptor semiconductor are typically dissolved in an organic solvent. In order to enable green hydrogen production and render OPV technology more sustainable and respectful of the environment, aqueous dispersions have become an interesting alternative for developing eco-friendly processes. Two main routes have been developed to synthesize organic semiconductor particles, namely miniemulsion[23,24] and nanoprecipitation methods.[25] We selected the miniemulsion concept due to its simplicity and versatility in producing well-defined particles. This approach is particularly useful for controlling the morphology of the donor/acceptor combination. Fullerene derivatives-based donor/acceptor composite particles prepared by miniemulsion adapt different types of morphology, but the core–shell morphology usually dominates, due to a higher surface energy of the acceptor compared to the one of the donor material, particularly when SDS is used as a surfactant.[26,27] During this process, donor and acceptor materials tend to segregate within the hydrophobic droplets of the miniemulsion, reducing the interfacial energy with water, while the organic solvent gradually evaporates. Due to their high surface energy, the fullerene derivatives tend to migrate into the core of the nanoparticles, while the other component forms a surrounding shell. This morphology allows good charge separation, stabilizes the interface and minimizes energy losses.[28,29] Thus, such particles are highly adaptable for various applications and can be used in devices like solar cells and as photocatalysts. However, while the core–shell morphology of fullerene derivatives-based composite nanoparticles offers benefits for the initial charge separation and interface stabilization, it is not the optimal morphology for reducing charge-carrier recombination, which can limit the devices' efficiencies.[30]

Therefore, to further enhance the efficiency and functionality of organic donor–acceptor systems, innovative strategies are required. One such strategy involves the deposition of metals on semiconductor materials, which has been shown in numerous studies to produce hybrid materials with significantly higher catalytic activity than unmodified semiconductors.[31,32] In this regard, the design of Janus particles stands out as a promising strategy for the development of multifunctional catalysts.

In this work, we designed donor–acceptor particles that combine the conjugated polymer poly[*N*-9′-heptadecanyl-2,7-carbazole-*alt*-5,5-(4,7-di-2-thienyl-2′,1′,3′-benzothiadiazole)] (PCDTBT) as a donor with the fullerene derivative [6,6]-phenyl-C_{61}-butyric acid methyl ester ($PC_{61}BM$) as an electron acceptor. These particles constitute the starting point for the development of nanohybrids and have been tested for their photocatalytic hydrogen evolution performance. Given PCDTBT's well-documented device characteristics, optoelectronic properties, and high photochemical stability,[33,34] its role as an effective light absorber is particularly advantageous, making it a promising material for sustainable energy applications.

Building on this foundation, we introduce here an approach for the preparation of original Janus particles, which, for the first time, combine organic donor–acceptor materials with plasmonic metals like platinum (Pt), gold (Au), and palladium (Pd), generated by bipolar electrodeposition. These noble metals can serve as co-catalysts, with platinum playing a critical role due to its exceptional catalytic activity, stability, and ability to facilitate HER.

Results and discussion

Previous studies have demonstrated the possibility to use an external electric field to asymmetrically modify a large number of conducting particles, dispersed in a dielectric medium, with metals by electrodeposition, but without the need for a direct contact with an electrode.[35] Alternatively, our group has explored the use of this so-called bipolar electrochemistry to generate more or less complex anisotropic structures, either based on conducting materials[36,37] or with semiconductor substrates such as TiO_2 nanofibers[38] and microspheres.[39] In the present study, we apply this concept for the site-selective deposition of metals on organic semiconductors to produce a large variety of Janus particles with controllable morphology, based on the synergy of light and the polarizing effect of an electric field. The resulting hybrid objects are then shown to be much more efficient in terms of photocatalytic hydrogen evolution compared to their randomly modified counterparts.

Bipolar electrochemistry is a wireless electrochemical process in which opposite electrochemical reactions occur simultaneously at the two extremities of a conducting support. The concept relies on the fact that when a conducting object is positioned in a solution under the influence of an electric field, a polarization of the two extremities of the object occurs. The associated polarization voltage difference with respect to the

solution, ΔV, is proportional to the electric field E, which represents the driving force, and the object's length d: $\Delta V = E \times d$.

If ΔV is sufficiently high, electrochemical reactions can take place simultaneously at both ends of the object, an oxidation reaction at the anodic pole and a reduction reaction at the cathodic pole.[40–43] However, this method cannot be directly applied to the modification of semiconductor materials due to their low intrinsic conductivity. To overcome this limitation, an additional light source is required to photogenerate charge carriers within the semiconductor, which are then driven into opposite directions by the external electric field, thus enhancing charge separation.

Under the simultaneous influence of light and electric field, the spatially asymmetric reduction of a metal precursor on an organic semiconductor, either present as a thin film or as particles, occurs as illustrated in Scheme 1. Two electrode compartments are connected by a channel which is filled with the reaction mixture containing an aqueous suspension of the metal salt and a PCDTBT:$PC_{61}BM$ thin film or particles (Fig. S1†). When an organic bulk heterojunction absorbs light having an energy exceeding the band gaps of either the donor or the acceptor (E_g), the exciton formed in the donor material will undergo an electron transfer from the LUMO of the donor to the LUMO of the acceptor. Conversely, a similar phenomenon happens for the exciton formed in the acceptor material. At the donor/acceptor interface, the holes transfer from the HOMO of the acceptor to the HOMO of the donor (Fig. S2†). Both phenomena will lead to a charge-separated state and free charges, electrons and holes, in the acceptor and donor phases, respectively.[44–46] The resulting electrons and holes migrate to the surface of the semiconductor, where they can initiate reactions with the redox active species in solution. If an electric field is simultaneously applied, it induces positive (δ^+) and negative (δ^-) polarization at the extremities of the semiconductor. This combination of the external electric field and the induced polarization causes band bending, creating an internal electric field that promotes the separation of electrons and holes and their transport to opposite sides of the particle, where reduction and oxidation reactions can take place. This mechanism introduces a notable difference compared to normal bipolar electrodeposition on classic conductors.[42,47] Normally, reduction occurs at the negatively polarized side of the object, which faces the feeder anode. However, in light-induced bipolar deposition, the reduction takes place at the positively polarized extremity of the semiconductor, which is oriented toward the feeder cathode.[48] Simultaneously, oxidation reactions take place at the opposite extremity, typically involving the oxidation of water.

Asymmetric modification of a macroscopic film

To illustrate this site-selective reduction of metal salts on organic bulk heterojunction materials, we carried out a first proof-of-principle experiment with a macroscopic film of PCDTBT:$PC_{61}BM$, spin-coated on a glass substrate (see ESI† for details), and hexachloroplatinic acid (H_2PtCl_6) as a metal precursor. The modified glass substrates were inserted in an aqueous solution of 1 mM H_2PtCl_6. After exposing the thin film to different conditions (only external electric field, only light or both simultaneously), the PCDTBT:$PC_{61}BM$ films were rinsed and subsequently analyzed by SEM (Fig. 1). When only an electric field is applied, the SEM image (Fig. 1a) shows no metal deposition, indicating that the electric field (2.8 kV m^{-1}) alone is insufficient to drive the reduction of metal ions. On the contrary, when the film was exposed solely to UV-visible light (mercury xenon source, 62 mW cm^{-2}, see ESI† for details), a random deposition of Pt particles on the entire surface of the organic film was observed (Fig. 1b). This suggests that light plays a critical role in initiating the reduction process. Finally, and most importantly, when both, an electric field of 2.8 kV m^{-1} and light were applied simultaneously, an asymmetric deposition of platinum was achieved (Fig. 1c), with bright platinum nanoparticles selectively deposited at the positively polarized edge of the film. This demonstrates the synergistic effect of light and electric field for controlling the spatial distribution of metal deposition, enabling a site-selective growth on the organic semiconductor. To get a better understanding of the dynamics of the asymmetric bipolar electrodeposition, we examined the influence of the electric field intensity on the deposition process.

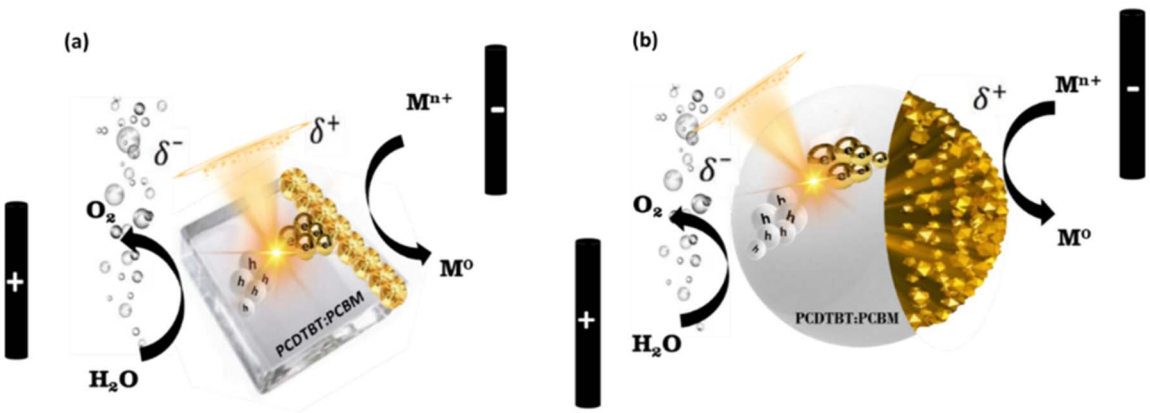

Scheme 1 Scheme of bipolar metal deposition on (a) a PCDTBT:$PC_{61}BM$ thin film and (b) a PCDTBT:$PC_{61}BM$ particle.

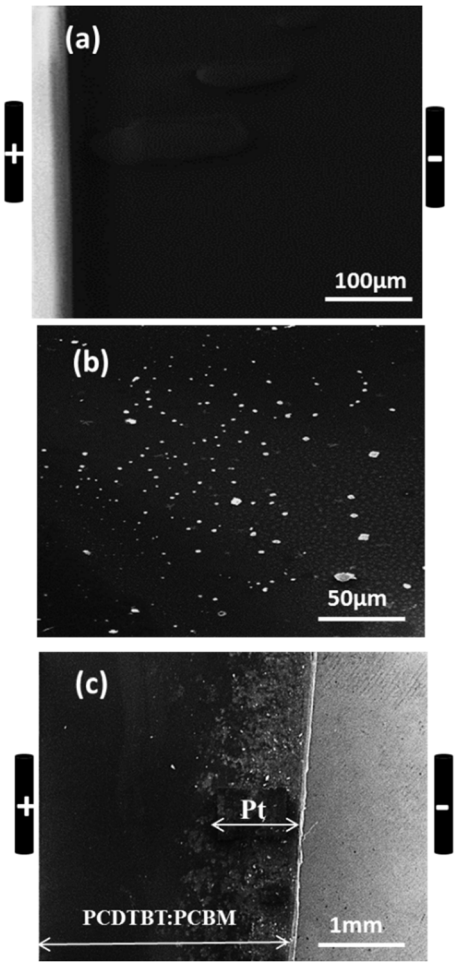

Fig. 1 SEM images of PCDTBT:$PC_{61}BM$ thin films after exposition (a) to only an external electric field, (b) only to light and (c) to light and an electric field of 2.8 kV m^{-1} for 2 min in the presence of an aqueous solution of 1 mM H_2PtCl_6.

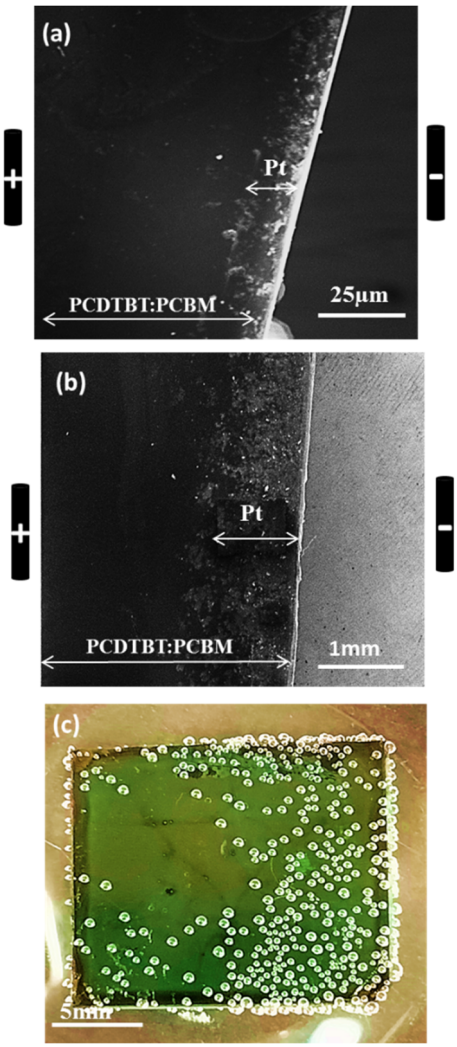

Fig. 2 SEM images of the asymmetric platinum deposit on a thin film of PCDTBT:$PC_{61}BM$ after simultaneous application of light (62 mW cm^{-2}) and an electric field of (a) 10 kV m^{-1}, (b) 2.8 kV m^{-1} (c) photograph of a hybrid film of Pt/PCDTBT:$PC_{61}BM$, synthesized at 0.7 kV m^{-1}, during photocatalytic water splitting, indicating the asymmetric reactivity by the inhomogeneous distribution of hydrogen bubbles.

Our results show that for a high electric field intensity (10 kV m^{-1}), the metal-decorated region is relatively narrow (~20 μm) as shown in Fig. 2a, whereas for lower electric fields (2.8 kV m^{-1}), the modified area is broader (~1 mm) as illustrated in Fig. 2b. This can be explained by the fact that a stronger electric field guides the charge carriers more efficiently towards the edge where metal reduction occurs, leading to a more focused deposition. Conversely, a weaker electric field leads to less directed electron movement, causing a larger deposition zone. These results demonstrate that site-selective modification arises from the synergy between light-induced electron–hole generation and the action of the charge-directing external electric field, resulting in a Janus film. To evaluate the photocatalytic efficiency of the Janus Pt/PCDTBT:$PC_{61}BM$ thin film for hydrogen production, a water-splitting experiment has been carried out, using ascorbic acid as a sacrificial agent (see ESI† for details).

As can be seen in Fig. 2c and in Video S1,† the amount of hydrogen bubbles produced at the Pt-decorated side of the Janus film (right part of the film) is significantly higher than at the undecorated side. This illustrates the important role of platinum as co-catalyst for enhancing the photocatalytic activity of PCDTBT:$PC_{61}BM$ by improving the separation of the photogenerated charge carriers. These findings validate that both, the choice of the organic material and the use of platinum as a co-catalyst, allow the design of a photoactive Janus film for hydrogen production.

Asymmetric modification of particles

Building up on this successful demonstration of asymmetric Pt deposition on a macroscopic film, using light-assisted bipolar electrochemistry, the deposition of metal was then investigated on PCDTBT:$PC_{61}BM$ particles and the resulting Janus nanohybrids were tested with respect to hydrogen generation. Binary donor–acceptor particles were synthesized using a miniemulsion process (see ESI† for details). The organic

components are first dissolved in chloroform, which is then mixed with an aqueous phase containing sodium dodecyl sulfate (SDS). An emulsion is obtained by submitting the mixture to high shear forces, generated by ultrasound, resulting in droplets of the organic phase dispersed in the aqueous phase. The emulsion is then submitted to a thermal treatment in order to evaporate the solvent, resulting in the formation of solid particles dispersed in water. In a subsequent centrifugation step, the excess of free surfactant is removed (see ESI† for details). This process is highly efficient for producing organic particles with controlled size and morphology.[10,49]

SEM images of SDS-stabilized PCDTBT:$PC_{61}BM$ particles (Fig. 3a) reveal an average size of about 525 nm, determined by dynamic light scattering (DLS, Table S1 and Fig. S3a†), and a smooth spherical morphology. The surfactant concentration significantly influences the particle size. Higher SDS concentrations lead to smaller particles (Fig. S3b†), while lower surfactant concentrations result in larger particles.[50,51] Moreover, decreasing the sonication power increases the particle size. In order to facilitate the imaging of the final hybrid particles and to better observe their structural details, we used larger particles for the following part of the study.

After the preparation of the PCDTBT:$PC_{61}BM$ particles, metal deposition was studied on these objects, dispersed in an aqueous 1 mM $H_2PtCl_6 \cdot 6H_2O$ solution containing agarose gel to create a viscous medium that prevents rotation of the particles during the modification experiment (see ESI† for details). Control experiments were conducted to ensure that light serves as the primary driving force for the deposition. When only light is applied, platinum nanoparticles are generated randomly over the entire surface of the organic semiconductor particles (Fig. 3b).

However, when both, an electric field and light, were applied simultaneously for 60 s to the particles, SEM images and EDS mapping clearly show that platinum is only present at one side of the particles (Fig. 3c and d), with approximately 70% of the particles being asymmetrically decorated. However, it is rather difficult to determine a very precise yield, because the only way is manual counting of the number of Janus particles present on an SEM image. Therefore, if for example the small metal deposit on a particle is facing the SEM substrate, the Janus character

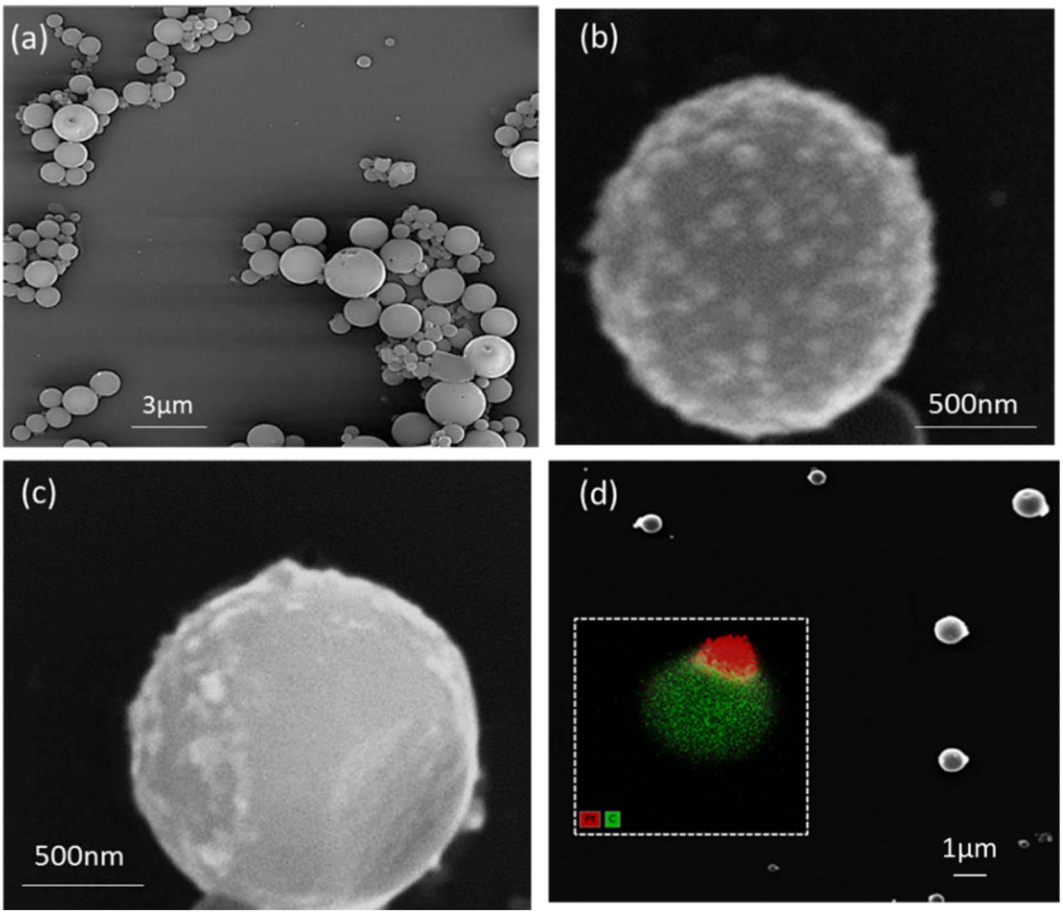

Fig. 3 SEM images of (a) PCDTBT:$PC_{61}BM$ particles synthesized by the miniemulsion method (40 mg ml^{-1} with 1 mg per ml SDS) (b) after Pt deposition with only light for 5 min or (c) under the simultaneous influence of an electric field of 10 kV m^{-1} and light irradiation for 60 s in a solution containing 1 mM $H_2PtCl_6 \cdot 6H_2O$. (d) SEM image with EDS mapping (C: green; Pt: red) of platinum deposited asymmetrically on PCDTBT:$PC_{61}BM$ particles by simultaneous exposure for 60 s to light and an electric field of 20 kV m^{-1} in a solution containing 1 mM $H_2PtCl_6 \cdot 6H_2O$.

will be hidden and thus the yield might be underestimated. Nevertheless, it is clear that the majority of the particles are modified and this highlights the crucial role of the electric field with respect to charge separation, as it guides the electrons, more or less efficiently as a function of its strength, towards the extremity where the metal reduction occurs.[48] As shown for the modification of the macroscopic PCDTBT:$PC_{61}BM$ thin films (*vide supra*), the amplitude of the electric field has a strong influence on the extension and the morphology of the metal deposit. This is also the case for particles, as illustrated in Fig. 3d, which has been recorded with particles that have experienced a two-fold increased electric field value (20 kV m^{-1}), leading to a more focused metal deposition compared to particles shown in Fig. 3c (10 kV m^{-1}). This is in strong contrast to what is expected for a normal bipolar electrodeposition process carried out with conducting particles, where a higher electric field would result in an extension of the modified area. This is due to the fact that, unlike in the classic process where the electric field acts as the essential driving force, in the present case it only helps to spatially guide the redox reactions and to enhance charge separation, whereas the ultimate driving force is provided by light *via* the band gap energy of the semiconductor. Consequently, experiments with semiconductors rely on the synergy between light and electric field.

Another point of interest is that, as explained before, compared to traditional bipolar electrodeposition, involving classic conductors such as carbon or metal, where the bipolar object is equipotential and the metal reduction typically occurs at the δ^- extremity, in the case of semiconductors the metal deposition occurs at the δ^+ site. This unusual behavior can be explained by the generation of an internal electric field within the semiconductor with an orientation opposite to the external one, which logically also inverts the deposition pattern. To further confirm this atypical behavior, various experimental parameters have been studied to illustrate its generic character and to demonstrate that the effect allows fine-tuning of the final composition and morphology of the Janus objects. First, the possibility of varying the nature of the metal by replacing the platinum precursor with gold and palladium salts was explored. Under the simultaneous application of light and an electric field, gold and palladium-coated Janus particles were successfully synthesized with metal deposition occurring exclusively on one side of the nanoparticle (Fig. 4b, c, e and f respectively). In strong contrast, when only light was applied without electric field, a uniform coating of randomly distributed metal nanoparticles was observed on the entire particle, as confirmed by EDS analysis in Fig. 4a and d. These results highlight the versatility of the process. Additional XPS studies (see Fig. S4–S6†) indicate that the deposits are mainly composed of metallic species Pt^0, Au^0 or Pd^0, confirming that the reduction process actually takes place whatever the nature of the metal. We furthermore investigated the effect of metal salt concentration on the deposition process. According to the SEM images shown in Fig. 4b and c, the amount of deposited gold becomes significantly higher when the $HAuCl_4 \cdot 3H_2O$ concentration is increased from 1 mM to 5 mM.

The effect of the amplitude of the electric field was a third parameter studied in a systematic way, and a series of experiments were conducted to better understand its influence. Bipolar electrodeposition of palladium was carried out by varying the applied electric field from 5 kV m^{-1} to 25 kV m^{-1}. It turns out that as the electric field increases, the decorated

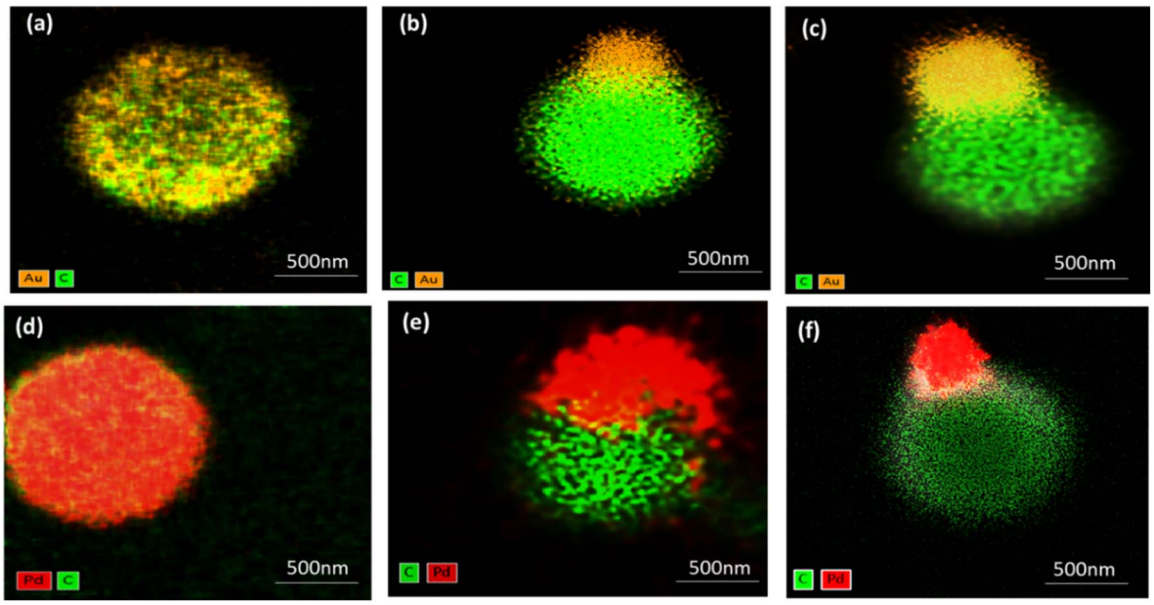

Fig. 4 EDS mapping (C: green; Au: orange) of gold deposition on PCDTBT:$PC_{61}BM$ particles, obtained (a) under light irradiation without electric field, (b and c) by simultaneous exposure to light and an electric field of 20 kV m^{-1} in a solution containing 1 mM or 5 mM $HAuCl_4 \cdot 3H_2O$, respectively. EDS mapping (C: green; Pd: red) of a palladium deposit on PCDTBT:$PC_{61}BM$ particles obtained (d) under light irradiation without electric field, (e and f) by simultaneous exposure for 60 s to light and an electric field of 5 kV m^{-1} or 25 kV m^{-1}, respectively, in a solution containing 1 mM $PdSO_4$.

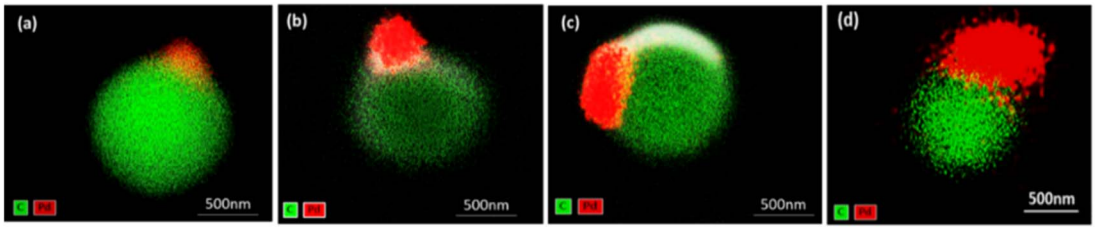

Fig. 5 EDS mapping (C: green; Pd: red) of asymmetric deposits of palladium on PCDTBT:$PC_{61}BM$ particles by simultaneous exposure to light and an electric field of 20 kV m^{-1} in a solution containing 1 mM of $PdSO_4$ for different deposition times (a) 30 s, (b) 60 s (c) 2 min and (d) 4 min.

surface area is more focused (Fig. 4e and f). This is due to the fact that a higher applied electric field more efficiently pushes the electrons to the extremities of the particles, like in the previous case of platinum (Fig. 3c and d). Last but not least, the effect of deposition time on the amount of deposited palladium was also investigated by applying light and the same intensity of the electric field for different times. EDS analysis indicates clearly that increasing the deposition time from 30 s to 4 min results in a higher amount of deposited metal (Fig. 5).

In conclusion of this part, the collection of results concerning the systematic variation of different experimental parameters clearly illustrates the possibility to tune at will the final composition and structure of organic semiconductor Janus particles with unprecedented precision. This should have a strong impact on their functionality, especially with respect to photocatalysis, which is examined in the following part of the work.

Photocatalytic hydrogen evolution

For the photocatalytic hydrogen generation, ascorbic acid has been used as a sacrificial agent in combination with three types of particles as photocatalysts: pure unmodified PCDTBT:PC_{61}BM nanoparticles, PCDTBT:PC_{61}BM nanoparticles randomly covered with platinum clusters synthesized by photodeposition, and Janus Pt/PCDTBT:PC_{61}BM nanoparticles prepared by light-assisted bipolar electrodeposition. For the latter case, the mechanism of gas formation is schematically illustrated in Fig. 6a.

A suspension of the selected nanoparticles (0.1 mg) was added to 2.5 ml of an aqueous solution containing 0.2 M of ascorbic acid (pH = 3), which acts as a sacrificial electron donor. The mixture was continuously stirred under UV-visible light irradiation (62 mW cm^{-2}) to initiate the water-splitting reaction, resulting in hydrogen bubble generation. The amount of produced hydrogen was quantified with a homemade hydrogen collection system based on water replacement (see Fig. S7†). Despite of being less precise compared to *e.g. in situ* gas chromatographic measurements, this simple, yet reliable set-up allowed us to obtain consistent results, providing sufficient first evidence of the considerably different performance of the various types of hybrid nanoparticles. It revealed that the Janus nanoparticles exhibited the highest photocatalytic efficiency, with a hydrogen production rate of 270 mmol h^{-1} g^{-1} to be compared with 62.4 mmol h^{-1} g^{-1} and 20.8 mmol h^{-1} g^{-1} for particles randomly covered with platinum and unmodified PCDTBT:PC_{61}BM nanoparticles, respectively. Although the exact amount of platinum present on each nanoparticle could not be measured, the hydrogen production results clearly indicate the superior efficiency of the Janus nanoparticles. This represents a significant increase of almost 500% compared to the randomly covered nanoparticles, which, in turn, surpass the performance of the unmodified PCDTBT:PC_{61}BM nanoparticles. This enhanced efficiency is also visible in the images and videos recorded during the experiments, where the quantity of released hydrogen bubbles is observed. As can be seen in Fig. 6b and Video S2,† the unmodified particles produce almost no hydrogen, whereas the ones decorated randomly with platinum exhibit an already slightly higher amount of hydrogen bubbles (Fig. 6c and Video S3†). Finally, the hydrogen release is the most pronounced for the Janus nanoparticles, as illustrated in Fig. 6d and Video S4,† under otherwise identical conditions. It is important to mention that during the photocatalytic water splitting experiments, performed continuously for over 3 hours, the catalyst particles exhibited excellent structural and chemical stability. No signs of aggregation, degradation, or chemical decomposition of the nanoparticles were observed.

The catalytic performance improvement, attributed to the asymmetric Pt decoration of the Janus nanoparticles, positions this concept as a promising approach to design organic photocatalysts, showing significant application potential. In comparison to other studies, our work indicates that organic photocatalysts, and especially those modified in an asymmetric way, are very interesting candidates for hydrogen production. Several recent studies have equally highlighted the potential of organic materials in this area.

For instance, Y. Yang *et al.*[52] developed PBDB-T/ITIC-based bulk heterojunction nanoparticles, produced *via* the micro-emulsion method, achieving a remarkable hydrogen evolution rate of 257 mmol h^{-1} g^{-1}. Similarly, H. Yang *et al.*[53] explored a variety of donor–acceptor nanohybrids (DANHs) combining conjugated polymer donors with fullerene or non-fullerene acceptors, screening a library of 237 organic nanohybrids. Their PCDTBT/PC_{60}BM system showed significant performance, with a hydrogen evolution rate of 105.2 mmol h^{-1} g^{-1}. These developments are complemented by another study,[54] reporting the incorporation a crystalline n-type small-molecule organic semiconductor (IDMIC-4F) into a binary host of PM6 and ITCC-M, leading to a ternary nanoparticle photocatalyst with an outstanding hydrogen evolution rate of 307 mmol h^{-1}

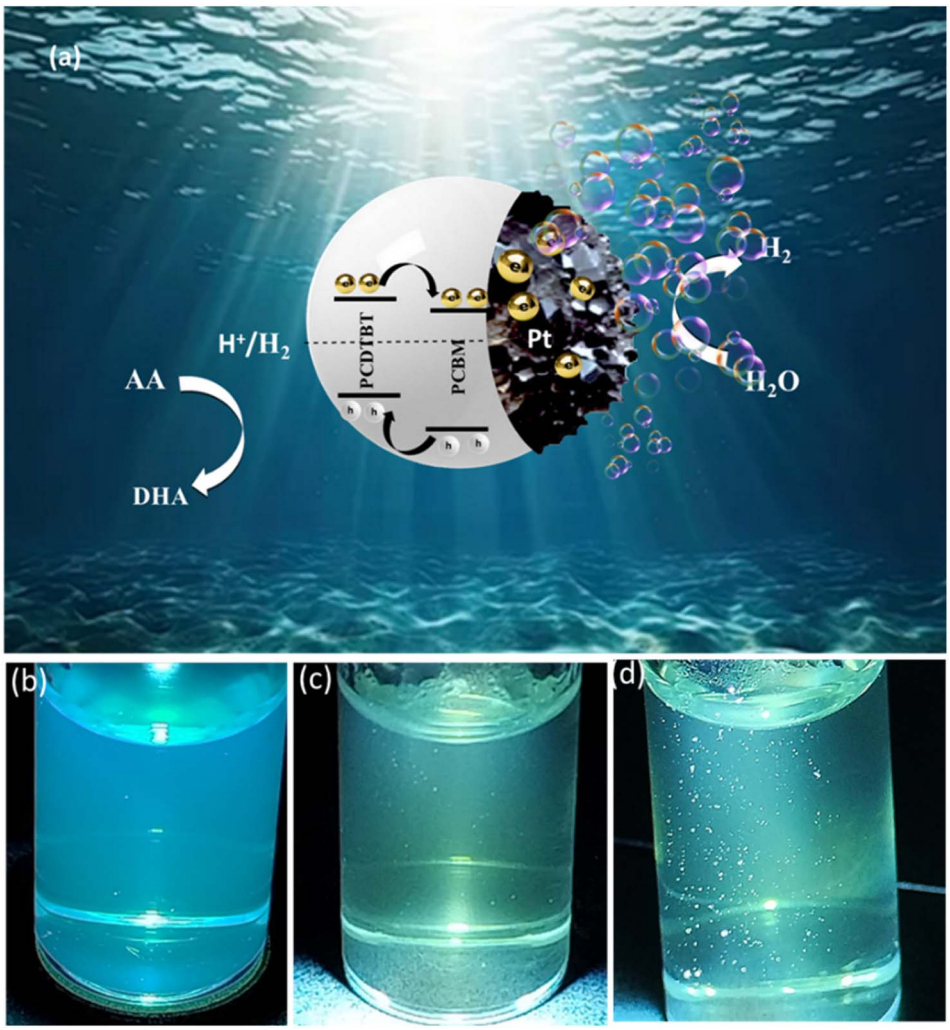

Fig. 6 Photocatalytic hydrogen evolution: (a) schematic illustration of the charge transfer mechanism related to hydrogen evolution at Janus Pt/PCDTBT:$PC_{61}BM$ nanoparticles under light irradiation. (b–d) Variation of the intensity of hydrogen bubble formation during the water splitting reaction using 0.2 M ascorbic acid (AA) as a sacrificial electron donor and 0.1 mg of (b) unmodified PCDTBT:PC61BM particles, (c) Pt/PCDTBT:$PC_{61}BM$ particles modified with Pt by photodeposition (d) Janus Pt/PCDTBT:$PC_{61}BM$ particles in 2.5 ml of aqueous solution.

g^{-1}. Compared to these very interesting systems, the Janus particles reported in this contribution, which exhibit a hydrogen evolution rate of 270 mmol h^{-1} g^{-1}, position themselves as very efficient organic photocatalysts, based on their unique asymmetric design which enhances charge separation.

This substantial increase in efficiency can be qualitatively attributed to three key factors: the crucial role of platinum as a co-catalyst,[55] its asymmetric deposition on the photoactive particles, and the use of organic semiconductors having a good light absorption capacity over a large range of wavelengths in the visible part of the solar spectrum (Fig. S8†).[56–58] Additionally, PCDTBT:PCBM, when used in bulk heterojunction solar cells, achieves an internal quantum efficiency approaching 100% and an external quantum efficiency on the order of 80%, as reported by Sung Heum Park and coworkers.[59] This remarkable performance highlights the exceptional feature that almost every absorbed photon leads to a separated pair of charge carriers, making this material not only a promising choice for solar cells, but also for hydrogen production. Moreover, platinum facilitates efficient proton reduction to hydrogen,[60,61] due to its low overpotential for this reaction, making its asymmetric deposition at just one face of the particles especially advantageous. By localizing platinum at one side, the directionality of electron flow is enhanced, effectively reducing the probability of electron–hole recombination. This spatial separation of charge carriers ensures that electrons are preferentially guided towards the platinum for hydrogen evolution, while the holes are scavenged at the opposite face of the nanoparticle by ascorbic acid.[52,62] An alternative explanation of the observed beneficial effect of the Janus architecture is that the localized deposition of Pt at one side of the Janus nanoparticles can significantly reduce optical shading, compared to a random distribution of the metal, which might block incident light, thus inhibiting its absorption by the semiconductor and, in turn, leading to a decrease of the photocatalytic performance. Both hypotheses

equally highlight the potential benefits offered by a well-controlled Janus configuration, which advantageously combines all key ingredients in an original way, significantly increasing their overall performance for hydrogen production. We can conclude that this unique combination of bulk heterojunction donor/acceptor semiconductors, which exhibit strong visible light absorption, high charge separation efficiency, and excellent charge mobility, with the proposed site-selective Pt decoration, results in an efficient and highly tunable system for the future development of green hydrogen technologies.

Conclusion

We successfully demonstrated the synthesis of metal/PCDTBT:$PC_{61}BM$ Janus particles (metal = Pt, Au, Pd) *via* a controlled deposition by light-assisted bipolar electrochemistry. A systematic study of key parameters such as the electric field intensity, the nature and concentration of the metal precursor, as well as the deposition time, revealed the possibility to fine-tune the composition and the morphology of the resulting hybrid metal–organic particles. In the case of the Pt-based Janus system, photocatalytic hydrogen evolution tests provide evidence that the Janus structure outperforms both randomly Pt-covered and pure organic particles, resulting in a five-fold increase in photocatalytic efficiency. This enhancement can be attributed to directional charge carrier separation and minimized recombination due to the asymmetric distribution of catalytically active platinum sites, and/or a reduced shading effect. Moreover, the synergy between the bulk heterojunction donor–acceptor system, and the site-selective metal deposition, greatly enhances exciton dissociation and facilitates electron transfer. Thus, this combination of organic semiconductors and targeted metal deposition leads to an efficient and highly tunable system for hydrogen production. Further, more precise *in situ* analysis of the produced amount of hydrogen will allow an even better understanding of the structure–performance relationship and enable additional optimization of these photocatalytic systems. However, already from these first proof-of-principle experiments, it becomes clear that this Janus particle design represents a promising step forward in the frame of the development of green hydrogen production technologies and also opens up new perspectives in the general context of the elaboration of advanced hybrid photocatalytic systems, offering significant potential for sustainable energy applications.

Data availability

The data that support the findings of this study are available from the corresponding author upon reasonable request.

Author contributions

K. Missaoui: investigation, methodology, analysis, writing – original draft. G. Wantz: conceptualization, funding acquisition, writing – review & editing. T. Toupance: conceptualization, supervision, funding acquisition, writing – review & editing. S. Chambon: conceptualization, supervision, writing – review & editing. A. Kuhn: conceptualization, supervision, funding acquisition, writing – review & editing.

Conflicts of interest

There are no conflicts to declare.

Acknowledgements

This study received financial support from the French Government in the framework of the University of Bordeaux's IdEx "Investments for the Future" program GPR PPM.

Notes and references

1 M. Grätzel, *Philos. Trans. R. Soc., A*, 2007, **365**, 993–1005.
2 Y. Gwon, S. Jo, H.-J. Lee, S. Y. Park and T. S. Lee, *Polymer*, 2021, **229**, 124004.
3 C. Cheng, B. He, J. Fan, B. Cheng, S. Cao and J. Yu, *Adv. Mater.*, 2021, **33**, 2100317.
4 X. Chen, S. Shen, L. Guo and S. S. Mao, *Chem. Rev.*, 2010, **110**, 6503–6570.
5 A. Kudo and Y. Miseki, *Chem. Soc. Rev.*, 2009, **38**, 253–278.
6 Y. Qu and X. Duan, *Chem. Soc. Rev.*, 2013, **42**, 2568–2580.
7 C. X. Kronawitter, L. Vayssieres, S. Shen, L. Guo, D. A. Wheeler, J. Z. Zhang, B. R. Antoun and S. S. Mao, *Energy Environ. Sci.*, 2011, **4**, 3889.
8 A. Holmes, H. Laval, M. Guizzardi, V. Maruzzo, G. Folpini, N. Barbero, E. Deniau, M. Schmutz, S. Blanc, A. Petrozza, G. M. Paternò, G. Wantz, S. Chambon, C. Lartigau-Dagron and A. Bousquet, *Energy Environ. Sci.*, 2024, **17**, 1107–1116.
9 A. Holmes, H. Laval, E. Deniau, M. Schmutz, S. Blanc, G. Wantz, S. Chambon, C. Lartigau-Dagron and A. Bousquet, *Sol. Energy Mater. Sol. Cells*, 2024, **266**, 112656.
10 H. Laval, A. Holmes, M. A. Marcus, B. Watts, G. Bonfante, M. Schmutz, E. Deniau, R. Szymanski, C. Lartigau-Dagron, X. Xu, J. M. Cairney, K. Hirakawa, F. Awai, T. Kubo, G. Wantz, A. Bousquet, N. P. Holmes and S. Chambon, *Adv. Energy Mater.*, 2023, **13**, 2300249.
11 L. Meng, Y. Zhang, X. Wan, C. Li, X. Zhang, Y. Wang, X. Ke, Z. Xiao, L. Ding, R. Xia, H.-L. Yip, Y. Cao and Y. Chen, *Science*, 2018, **361**, 1094–1098.
12 Y. Cui, H. Yao, B. Gao, Y. Qin, S. Zhang, B. Yang, C. He, B. Xu and J. Hou, *J. Am. Chem. Soc.*, 2017, **139**, 7302–7309.
13 Y. Wang, A. Vogel, M. Sachs, R. S. Sprick, L. Wilbraham, S. J. A. Moniz, R. Godin, M. A. Zwijnenburg, J. R. Durrant, A. I. Cooper and J. Tang, *Nat. Energy*, 2019, **4**, 746–760.
14 S. Zhang, L. Ye and J. Hou, *Adv. Energy Mater.*, 2016, **16**, 1502529.
15 C. M. Aitchison, S. Gonzalez-Carrero, S. Yao, M. Benkert, Z. Ding, N. P. Young, B. Willner, F. Moruzzi, Y. Lin, J. Tian, P. D. Nellist, J. R. Durrant and I. McCulloch, *Adv. Mater.*, 2024, **36**, 2300037.
16 Y. Xu, M. Fan, W. Yang, Y. Xiao, L. Zeng, X. Wu, Q. Xu, C. Su and Q. He, *Adv. Mater.*, 2021, **33**, 2101455.

17 B. C. M. Martindale, E. Joliat, C. Bachmann, R. Alberto and E. Reisner, *Angew. Chem., Int. Ed.*, 2016, **55**, 9402–9406.
18 B. C. M. Martindale, G. A. M. Hutton, C. A. Caputo and E. Reisner, *J. Am. Chem. Soc.*, 2015, **137**, 6018–6025.
19 C. Shu, C. Han, X. Yang, C. Zhang, Y. Chen, S. Ren, F. Wang, F. Huang and J. Jiang, *Adv. Mater.*, 2021, **33**, 2008498.
20 L. Liu, M.-Y. Gao, H. Yang, X. Wang, X. Li and A. I. Cooper, *J. Am. Chem. Soc.*, 2021, **143**, 19287–19293.
21 J. Bisquert, P. Cendula, L. Bertoluzzi and S. Gimenez, *J. Phys. Chem. Lett.*, 2014, **5**, 205–207.
22 T. M. Clarke and J. R. Durrant, *Chem. Rev.*, 2010, **110**, 6736–6767.
23 T. Kietzke, D. Neher, M. Kumke, R. Montenegro, K. Landfester and U. Scherf, *Macromolecules*, 2004, **37**, 4882–4890.
24 T. Kietzke, D. Neher, K. Landfester, R. Montenegro, R. Güntner and U. Scherf, *Nat. Mater.*, 2003, **2**, 408–412.
25 S. Gärtner, M. Christmann, S. Sankaran, H. Röhm, E. Prinz, F. Penth, A. Pütz, A. E. Türeli, B. Penth, B. Baumstümmler and A. Colsmann, *Adv. Mater.*, 2014, **26**, 6653–6657.
26 N. P. Holmes, S. Chambon, A. Holmes, X. Xu, K. Hirakawa, E. Deniau, C. Lartigau-Dagron and A. Bousquet, *Curr. Opin. Colloid Interface Sci.*, 2021, **56**, 101511.
27 A. Holmes, E. Deniau, C. Lartigau-Dagron, A. Bousquet, S. Chambon and N. P. Holmes, *ACS Nano*, 2021, **15**, 3927–3959.
28 V. Chiozzi and F. Rossi, *Nanoscale Adv.*, 2020, **2**, 5090–5105.
29 M.-P. Zhuo, X.-D. Wang and L.-S. Liao, *Mater. Horiz.*, 2020, **7**, 3161–3175.
30 J. Kosco, M. Bidwell, H. Cha, T. Martin, C. T. Howells, M. Sachs, D. H. Anjum, S. G. Lopez, L. Zou, A. Wadsworth, W. Zhang, L. Zhang, J. Tellam, R. Sougrat, F. Laquai, D. M. DeLongchamp, J. R. Durrant and I. McCulloch, *Nat. Mater.*, 2020, **19**, 559–565.
31 Z. Zheng, B. Huang, X. Qin, X. Zhang, Y. Dai and M.-H. Whangbo, *J. Mater. Chem.*, 2011, **21**, 9079.
32 M. A. Hajjaji, K. Missaoui, K. Trabelsi, A. Bouzaza, A. Hajjaji, B. Bessais and A. A. Assadi, *J. Photochem. Photobiol., A*, 2025, **458**, 115975.
33 E. A. Parlak, T. Aslı Tumay, N. Tore, Ş. Sarıoğlan, P. Kavak and F. Türksoy, *Sol. Energy Mater. Sol. Cells*, 2013, **110**, 58–62.
34 S. Cheruku, L. D'Olieslaeger, N. Smisdom, J. Smits, D. Vanderzande, W. Maes, M. Ameloot and A. Ethirajan, *Materials*, 2019, **12**, 2497.
35 Y. Koizumi, N. Shida, I. Tomita and S. Inagi, *Chem. Lett.*, 2014, **43**, 1245–1247.
36 G. Loget, J. Roche and A. Kuhn, *Adv. Mater.*, 2012, **24**, 5111–5116.
37 P. Chassagne, P. Garrigue and A. Kuhn, *Adv. Mater.*, 2024, **36**, 2307539.
38 M. Ongaro, J. Roche, A. Kuhn and P. Ugo, *ChemElectroChem*, 2014, **1**, 2048–2051.
39 S. Tiewcharoen, C. Warakulwit, V. Lapeyre, P. Garrigue, L. Fourier, C. Elissalde, S. Buffière, P. Legros, M. Gayot, J. Limtrakul and A. Kuhn, *Angew. Chem.*, 2017, **129**, 11589–11593.
40 G. Loget, D. Zigah, L. Bouffier, N. Sojic and A. Kuhn, *Acc. Chem. Res.*, 2013, **46**, 2513–2523.
41 N. Shida, Y. Zhou and S. Inagi, *Acc. Chem. Res.*, 2019, **52**, 2598–2608.
42 S. E. Fosdick, K. N. Knust, K. Scida and R. M. Crooks, *Angew. Chem., Int. Ed.*, 2013, **52**, 10438–10456.
43 L. Koefoed, S. U. Pedersen and K. Daasbjerg, *Curr. Opin. Electrochem.*, 2017, **2**, 13–17.
44 K. A. Mazzio and C. K. Luscombe, *Chem. Soc. Rev.*, 2015, **44**, 78–90.
45 G. J. Hedley, A. Ruseckas and I. D. W. Samuel, *Chem. Rev.*, 2017, **117**, 796–837.
46 H.-L. Yip and A. K.-Y. Jen, *Energy Environ. Sci.*, 2012, **5**, 5994.
47 L. Bouffier, D. Zigah, N. Sojic and A. Kuhn, in *Electroanalytical Chemistry*, CRC Press, 2017, pp. 27–118.
48 A. A. Melvin, E. Lebraud, P. Garrigue and A. Kuhn, *Phys. Chem. Chem. Phys.*, 2020, **22**, 22180–22184.
49 A. J. Bard and C. G. Zoski, *Electroanalytical Chemistry*, CRC Press, 2017.
50 O. Ghazy, B. Freisinger, I. Lieberwith and K. Landfester, *Nanoscale*, 2020, **12**, 22798–22807.
51 F. J. M. Colberts, M. M. Wienk and R. A. J. Janssen, *ACS Appl. Mater. Interfaces*, 2017, **9**, 13380–13389.
52 Y. Yang, D. Li, P. Wang, X. Zhang, H. Zhang, B. Du, C. Guo, T. Wang and D. Liu, *Polymer*, 2022, **244**, 124667.
53 H. Yang, X. Li, R. S. Sprick and A. I. Cooper, *Chem. Commun.*, 2020, **56**, 6790–6793.
54 Y. Yang, D. Li, J. Cai, H. Wang, C. Guo, S. Wen, W. Li, T. Wang and D. Liu, *Adv. Funct. Mater.*, 2023, **33**, 2209643.
55 P. Kumar, R. Boukherroub and K. Shankar, *J. Mater. Chem. A*, 2018, **6**, 12876–12931.
56 J. W. Mok, Z. Hu, C. Sun, I. Barth, R. Muñoz, J. Jackson, T. Terlier, K. G. Yager and R. Verduzco, *Chem. Mater.*, 2018, **30**, 8314–8321.
57 L. Lu, T. Zheng, Q. Wu, A. M. Schneider, D. Zhao and L. Yu, *Chem. Rev.*, 2015, **115**, 12666–12731.
58 C. Li, J. Zhou, J. Song, J. Xu, H. Zhang, X. Zhang, J. Guo, L. Zhu, D. Wei, G. Han, J. Min, Y. Zhang, Z. Xie, Y. Yi, H. Yan, F. Gao, F. Liu and Y. Sun, *Nat. Energy*, 2021, **6**, 605–613.
59 S. H. Park, A. Roy, S. Beaupré, S. Cho, N. Coates, J. S. Moon, D. Moses, M. Leclerc, K. Lee and A. J. Heeger, *Nat. Photonics*, 2009, **3**, 297–302.
60 J. Kosco, M. Sachs, R. Godin, M. Kirkus, L. Francas, M. Bidwell, M. Qureshi, D. Anjum, J. R. Durrant and I. McCulloch, *Adv. Energy Mater.*, 2018, **8**, 1802181.
61 J. R. McKone, S. C. Marinescu, B. S. Brunschwig, J. R. Winkler and H. B. Gray, *Chem. Sci.*, 2014, **5**, 865–878.
62 J. M. de la Perrelle, A. Dolan, E. R. Milsom, T. D. Small, G. F. Metha, X. Pan, M. R. Andersson, D. M. Huang and T. W. Kee, *J. Phys. Chem. C*, 2022, **126**, 14518–14528.